ACS Photonics

pubs.acs.org/journal/apchd5

Article

Quantum Coherence of Excitons Strongly Bound to the Magnetic Order

Sean Knapp, Arup Barua, Chevy Boegel, Shirin Mozaffari, Matthew Cothrine, David Mandrus, Dmitry Semenov, Stephen A. McGill, Aldo H. Romero, Nihar Pradhan, and Denis Karaiskaj*

Cite This: *ACS Photonics* 2025, 12, 5921−5928

Read Online

ACCESS | Metrics & More | Article Recommendations | Supporting Information

ABSTRACT: Excitons in $NiPS_3$ have shown very strong coupling to the antiferromagnetic order and exceedingly sharp photoluminescence line width, indicating very long quantum coherence. A long excitonic coherence has been inferred so far but never measured directly. Here, we start by investigating the substructure of the excitonic transition using high magnetic fields and confirm the nature of the different spectral components observed and strong coupling to the magnetic order. We conclude that the subcomponents of the excitonic transition originate from the three equivalent orientations of the Neel vectors. Surprisingly, these transitions are shifted energetically and are independent of each other. We perform four-wave mixing experiments and measure the excitonic dephasing rate at ∼20 ps, which corresponds to a homogeneous line width of <20 μeV. To further investigate the coherence time observed, the radiative lifetime of the excitons is measured. The radiative lifetime is half that of the excitonic coherence and is thought to be the limiting factor in setting the upper limit of the coherence time.

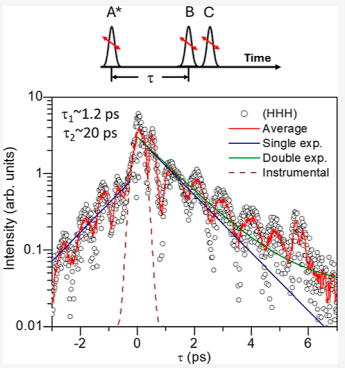

KEYWORDS: *nonlinear optical spectroscopy, four-wave mixing spectroscopy, two-dimensional excitons, antiferromagnets, layered magnetic materials*

INTRODUCTION

Antiferromagnets are promising materials for spintronics due to their terahertz frequency resonance and insensitivity to stray fields. However, the zero net magnetic moment of antiferromagnets makes the detection of the magnetic signals and the investigation of fundamental spin properties challenging due to large exchange interaction energies. Optical methods have been suggested as means to read the magnetic order in antiferromagnets, giving rise to new research efforts in magnetism known as antiferromagnetic opto-spintronics. Thus, insulating or ideally semiconducting antiferromagnets with band gaps in the optical or near-infrared range that form excitonic transitions are very desirable.[1] The Coulomb interactions governing excitons, i.e., bound electron−hole pairs, provide an efficient way to coupling to light fields.

Recently, the observation of excitons coupled to zigzag antiferromagnetic order[2−4] in the layered antiferromagnetic insulator $NiPS_3$ has been reported.[5] This exciton exhibits a very narrow photoluminescence line width of roughly 350 μeV, which is highly linearly polarized.[6] The emission is suppressed when the sample thickness is reduced from five to two layers and eventually vanishes for the monolayer. The degree of linear polarization observed in the photoemission spectra suggests strong coupling to the antiferromagnetic order.[7,8] This is further supported by the disappearance of the photoluminescence when approaching the Néel temperature of 150 K, even at somewhat lower temperatures.[9]

Several models have been proposed that would account for the observed properties of excitons in $NiPS_3$.[5,10−12] These excitons are thought to represent a spin−orbit-entangled state which arises intrinsically from the many-body states of the Zhang−Rice singlet which reaches a coherent state assisted by the antiferromagnetic order.[13] The origin of the excitonic state was attributed to a transition from a Zhang−Rice triplet to a Zhang−Rice singlet.[5] Excitons in strongly correlated magnetic materials have been observed, but the underlying mechanisms differ. Similar spin−orbit excitons, where the excitation between different J states is dressed by magnons, were discussed in Sr_2IrO_4 and α-$RuCl_3$.[14,15] This assignment was supported by theoretical calculations and experimentally by optical spectroscopy and resonant inelastic X-ray scattering. A more recent study finds that Hund's exchange interactions are primarily responsible for the energy of formation of the exciton.[12] The dispersion of the exciton was thought to indicate a propagation analogous to that of a double magnon. However, both of these models do not address the possible

Received: May 28, 2025
Revised: October 27, 2025
Accepted: October 31, 2025
Published: November 6, 2025

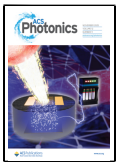

https://doi.org/10.1021/acsphotonics.5c01214
ACS Photonics 2025, 12, 5921−5928

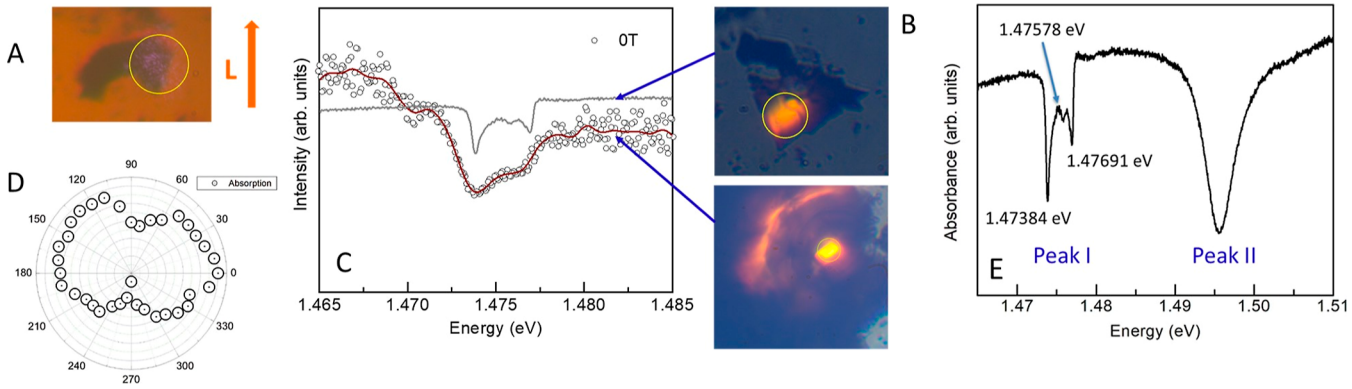

Figure 1. (A) Bulk $NiPS_3$ flake 1 used in the high magnetic field and four-wave mixing experiments. (B) Thinner bulk flake 2 used to resolve the subcomponents of the excitonic transition in $NiPS_3$. (C) Absorption spectra originating from (circles) flake 1 and (gray line) flake 2. (D) Absorption intensity as a function of polarization angle to determine the Néel vector. This corresponds to the most resolved excitonic subcomponent. The lowest intensity is obtained when the polarization vector of the incoming light is perpendicular to the Néel vector. The intensity pattern of the other components is rotated by 60° and 120°, respectively. (E) Absorption measurement of the excitonic region in $NiPS_3$ originating from flake 2. We observe two peaks labeled peak I and peak II. Peak I has been assigned to the excitonic region, whereas peak II is thought to be its two magnon replica. Peak I is composed of three resolved subcomponents.

role of Coulomb interactions and the mechanism of the strong coupling to light of these excitons.

The discussion of the magnetic exciton as a purely triplet-singlet excitation leaves open the question of how this excitation couples to the light field and how the optical selection rules are satisfied. In fact, recent studies have observed strong coupling to the light field and the formation of polaritons with unique signatures of excitons, photons, and spins.[16] Their theoretical analysis of strongly correlated electronic states in $NiPS_3$ based on an extended Hubbard model reveals excitonic transitions between sulfur p orbitals with zero net-magnetization and spin-polarized long-range ordered nickel d orbitals. Thus, these excitons intrinsically couple to the magnetic order of nickel spins. Furthermore, DFT calculations reveal strongly localized and tightly bound excitons by Coulomb interactions with a Bohr radius <1 nm that interact weakly with each other and as a result have very large saturation density.[17,18] The modest Rabi splitting in microcavities indicated a relatively low exciton oscillator strength. Finally, the narrow line width observed in photoluminescence measurements indicates a narrow homogeneous line width and long excitonic coherence, supported by early experiments.[5]

RESULTS AND DISCUSSION

Here, we perform a direct measurement of the excitonic coherence on $NiPS_3$ using four-wave mixing spectroscopy. Absorption spectroscopy on a thin bulk layer sample revealed a triplet structure of the main exciton line. Temperature- and high magnetic field-dependent absorption measurements indicate that the three components do not originate from the same excitonic center but are likely due to excitons belonging to the three equivalent orientations of the zigzag spin alinement, which lead to three energetically shifted excitons. We apply magnetic fields up to 25 T to realign the Néel vector with respect to the polarization of the incoming light. Depending on the alignment of the Néel vector with respect to the polarization of the incoming light, the subcomponents of the exciton can become equal strength or be canceled completely. Tightly bound excitons tend to have short radiative lifetime and coherence time. However, the coherence time of the excitonic transition in $NiPS_3$ was measured to be ∼20 ps, corresponding to a homogeneous line width of ∼33 μeV. Further measurements of the radiative lifetime reveal the limits to the coherence time.

We exfoliated several flakes of $NiPS_3$ of different thicknesses on quartz substrates. $NiPS_3$ single crystals were prepared by the chemical vapor transport method as described in ref 19. Two flakes were used for the present work. Flake 1 shown in Figure 1A is larger and thicker and is used for measurements at high magnetic fields. Flake 2 shown in Figure 1B is thinner and is used to resolve the full substructure of the exciton line. Absorption spectra from both flakes are shown in Figure 1C. The lines are broader for flake 1 due to some increased inhomogeneous broadening caused by the larger thickness of the sample. The absorption intensity of the excitonic line is expected to maximize when the Néel vector is perpendicular to the polarization of incoming light. We plot the intensity of the most dominant exciton absorption line as a function of the polarization angle in Figure 1D for the strongest, best resolved subcomponent. The intensity pattern of the other components is rotated by 60° and 120°, respectively.

The absorption measurements originating from flake 2 are shown in Figure 1E, where we observe two centers labeled previously as peak I and peak II. Peak I is the main exciton transition, whereas peak II is thought to be a two-magnon replica of peak I.[5] The absorption spectra of $NiPS_3$ reveal a triplet state for main exciton peak I. A closer analysis of the line shape reveals significant inhomogeneous broadening of the transitions. Gaussian fitting of the components reveals <0.5 meV line widths that are still predominantly inhomogeneously broadened. The homogeneous line width and the coherence time are thus well masked by the inhomogeneous broadening due likely to the impurities, defects, and strain fields.

In order to understand the substructure of the excitonic transition, we perform temperature- and magnetic field-dependent measurements up to 25 T. First, we explore if the three transitions we observe belong to the same center. Ground state to excited state splitting of excitons is often accompanied by an intensity ratio change of the transitions with increasing temperature. Such a change is not observed in our measurements or previous published work.[5,10] However, excitons belonging to three equivalent Néel vectors are

https://doi.org/10.1021/acsphotonics.5c01214
ACS Photonics 2025, 12, 5921−5928

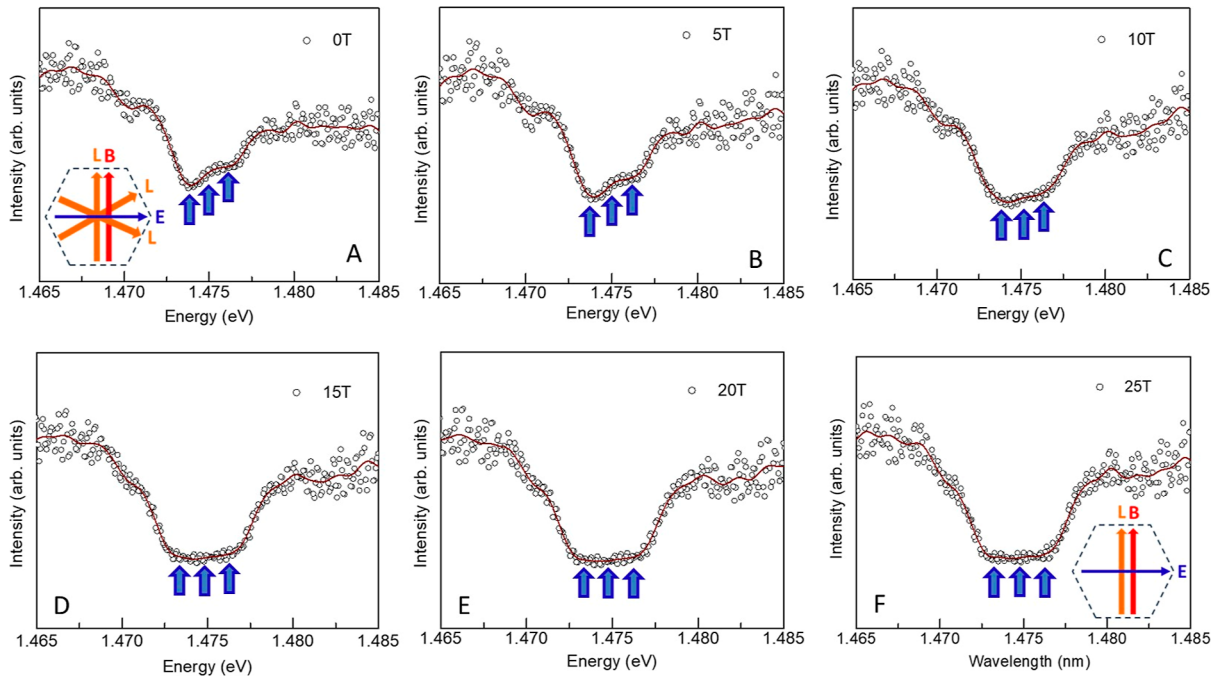

Figure 2. (A–F) High magnetic field absorption measurements originating from flake 1. We start at zero external magnetic field (A) and apply the magnetic field B and light polarization E perpendicular to each other. Initially, the Néel vectors are aligned along the three equivalent directions. With increasing magnetic fields from 5 T to 15 T (B–D), the Néel vectors are tilted toward the B field and perpendicular to the light polarization vector E. At the maximum field of 25 T, (F) the Néel vectors are fully aligned with the B field and perpendicular to the E vector. The three subcomponents marked by the blue arrows become equal strength. The three subcomponents are not well resolved in flake 1 due to its thickness.

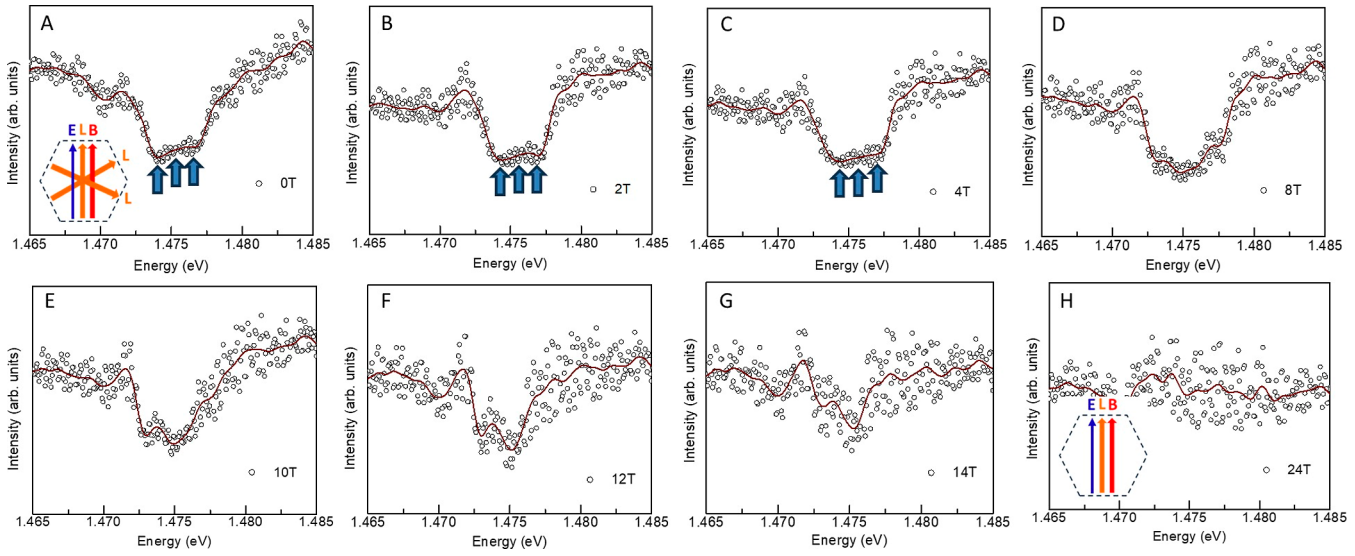

Figure 3. (A–H) High magnetic field absorption measurements originating from flake 1. We start at the zero external magnetic field (A) and apply the magnetic field B and light polarization E parallel to each other. Initially, the Néel vectors are aligned along the three equivalent directions. With increasing magnetic fields from 2 T to 14 T, (B–G) the Néel vectors are tilted toward the B field and parallel to the light polarization vector E. Above 14 T, the Néel vectors are aligned parallel to the light polarization vector E, leading to a complete cancelation of the absorption.

expected to be energetically degenerate. The intensity of the absorption depends on the angle between the light polarization E and the Néel vector N, but the energetic position is expected to be independent.

To further investigate the nature of the excitonic subcomponents, we performed magnetic field-dependent measurements.[20] We aligned our sample according to the assessment of the Néel vector shown in Figure 1A. We start with the light polarization perpendicular to the external magnetic field and perform absorption measurements up to 25 T. Due to the higher inhomogeneous broadening in the thicker and larger flake 1, only two subcomponents are clearly resolved, but we mark the spectral position of the three subcomponents fully resolved in the thinner flake 2 by three blue arrows. In the absence of magnetic fields, the intensity ratios of the peaks correspond to the spectra shown in Figure 1C, where the two outer lines are stronger. The data are shown in Figure 2 in 5 T increments of the magnetic field all the way

https://doi.org/10.1021/acsphotonics.5c01214
ACS Photonics 2025, 12, 5921–5928

to 25 T. As the external magnetic field increases, the intensity of the weaker components increases and at 15 T and above the three components become equal strength.

We continue with our magnetic field-dependent measurements and align the light polarization vector E parallel to the external magnetic field B. We measure the excitonic absorption for different applied magnetic fields, and data are shown in Figure 3A–H. As the Néel vectors L are tilted toward the external magnetic field B, at ∼14 T, the absorption disappears due to the L vector alinement being parallel with the polarization vector E. The arrangements of the different vectors at the low magnetic field and at the maximum field are shown in the insets of Figure 3A,H, respectively. This observation further support the temperature-dependent measurements which did not show intensity ratio changes between the subcomponents with increasing temperature. Assuming that the subcomponents originate from three different excitons, the magnetic field behavior of the excitonic subcomponents could be associated with the three equivalent directions of the Néel vectors. Starting at 15 T and all the way to the maximum magnetic field of 25 T, Néel vectors L are fully aligned with magnetic field B. They are aligned perpendicular to light polarization E, as shown in the inset of Figure 3H, and no absorption can be observed.

We performed a systematic theoretical analysis based on linear spin wave theory (LSWT), which included the Heisenberg exchange, Dzyaloshinskii–Moriya interactions, and symmetric anisotropic exchange couplings. This model enforces excitonic degeneracy, consistent with our finding that the exchange integrals are isotropic. However, LSWT neglects higher-order effects (magnon–magnon interactions and longitudinal fluctuations) and does not include single-ion anisotropy, interlayer coupling beyond bilinear exchange, or magnetoelastic/strain effects. The experimental observation of three distinct excitonic peaks and their polarization dependence under magnetic fields point to additional anisotropies outside our present model. In exfoliated monoclinic $NiPS_3$ flakes supported on substrates, such anisotropies can lift the degeneracy between zigzag domains and yield the meV-scale splitting we observe.

We measured the coherence and radiative lifetime of the excitonic center using nonlinear spectroscopy. Since the three excitonic subcomponents are thought to be associated with three equivalent Néel vectors L, we do not expect their dynamic properties to differ from each other. The technique we employ is based on the third-order response ($\chi^{(3)}$) requiring three light fields to generate a fourth field, the four-wave mixing (FWM) signal.[21,22] The three laser pulses A*, B, and C were focused on the sample held at 10 K centered inside the cryostat and are separated by the time delays τ and T, generating a FWM signal in the phase-matching direction $-k_A + k_B + k_C$. Two different polarization sequences presented, (H,H,H) and ($\sigma^+\sigma^+\sigma^+$) labeled here as colinear and cocircular. Linear polarizations excite both spin orientations, whereas the circular polarizations excite only one spin, which can have an effect on the observed dynamics. The time delay τ between the A* and B/C pulses measures the coherence or dephasing time, whereas the time delay T between the A*/B and C pulses measures the population decay or radiative recombination.[20,23–34] The spectral width of the laser pulse allows for the simultaneous excitation of all the excitonic states within peak I, excluding the two-magnon replica peak II which falls outside the laser spectrum.

The marginal third-order response is in agreement with theoretical calculations predicting tightly bound (Bohr radius, $a_B \approx 0.6$ nm) and weakly interacting excitons. We start our discussion with the colinear laser pulse sequence shown in Figure 4. We maintain pulses B and C at temporal overlap and

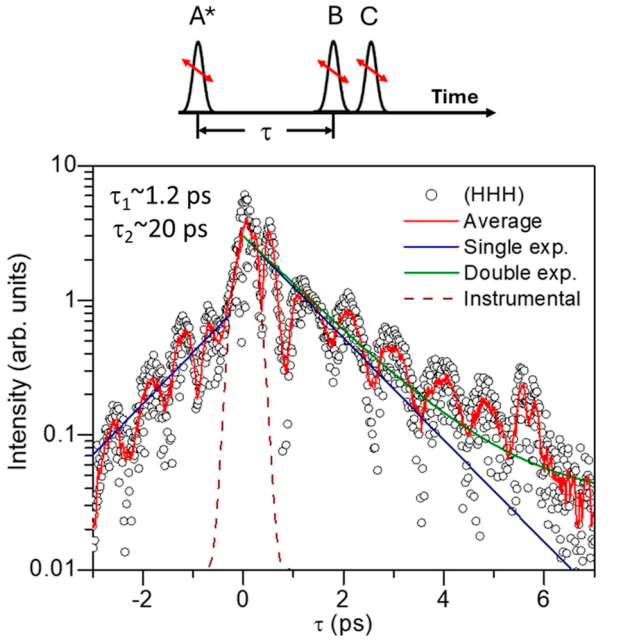

Figure 4. Four-wave mixing measurement using three linearly polarized laser pulses resonantly tuned to the exciton energy. When scanning the time delay τ between pulses A* and B, the dephasing time is measured. The exponential decays are used to fit the dephasing decay. The single exponential (blue line) fits well the initial part of the dephasing decay but fails to reproduce the later part of the dynamics. The double exponential (green line) includes a much longer decay component and fits the entire decay. The time constant for the shorter decay is $\tau_1 \sim 1.2$ ps, whereas the time constant for the longer decay is $\tau_2 \sim 20$ ps. The circles are the experimental data. The periodic oscillations correspond to a full period of ∼0.85 ± 0.05 ps and have been attributed to coherent magnons.

scan the time delay τ between pulses A* and B to measure the decoherence or dephasing time. The dephasing decay in Figure 4 is fit by using single and double exponential decay functions. The single exponential fit reproduces well the first part of the dephasing but fails to reproduce the later part at longer decays. The double exponential fit contains a decay component with a much longer time constant and reproduces well the entire dephasing dynamics. The two time constants corresponding to each exponential decay are $\tau_1 \sim 1.2$ ps and $\tau_2 \sim 20$ ps.

Furthermore, we observe oscillations with a period of ∼0.85 ps, corresponding to an energy of ∼5 meV. This is well in agreement with the optically active coherent magnon observed previously in pump–probe measurements.[35–37] The period of the oscillations does not agree with the energy separation of the excitonic subcomponents of 1.13 and 1.94 meV, respectively.[38–41] Another coherent magnon mode at ∼1.2 meV observed previously could not be observed in our experiment likely due to different excitation and detection methods.[7] Furthermore, the excitonic subcomponent was assigned to independent excitons that do not share the same ground state.[33,42] The instrumental response shown by the dashed line in Figure 4 rises much faster than what is observed

https://doi.org/10.1021/acsphotonics.5c01214
ACS Photonics 2025, 12, 5921–5928

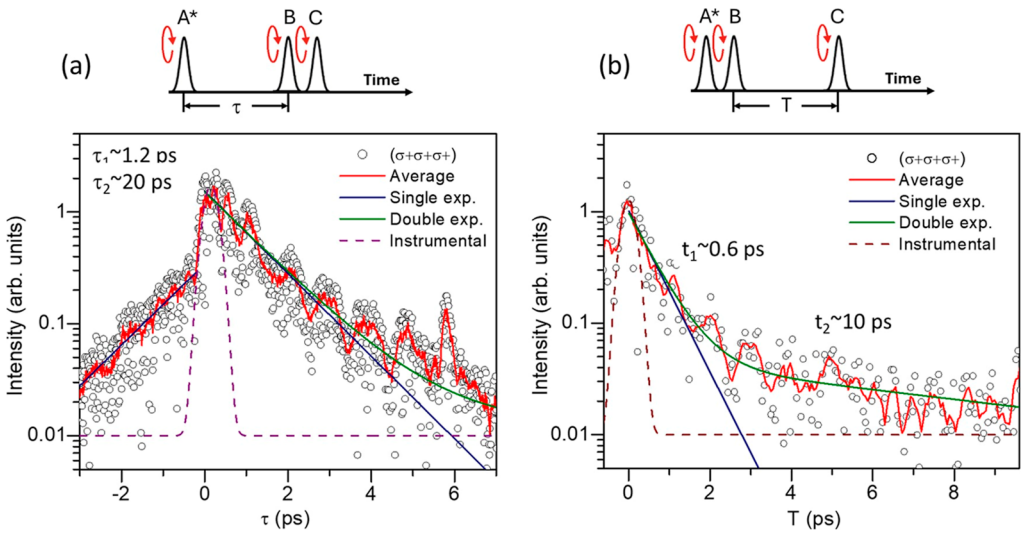

Figure 5. Four-wave mixing measurement using three circularly polarized laser pulses resonantly tuned to the exciton energy. (A) When scanning the time delay τ between pulses A* and B, the dephasing time is measured. The same double exponential dephasing with time constants $\tau_1 \sim 1.2$ ps and $\tau_2 \sim 20$ ps as in the linearly polarized case is observed. The periodic oscillations observed become much weaker for circularly polarized laser pulses likely due to selection rules in exciting coherent magnons. The residual oscillations observed are likely due to small ellipticity in the polarization of the laser pulses. (B) When scanning the time delay T between pulses B and C, the radiative lifetime is measured. The single exponential (blue line) fits well the initial part of the dephasing decay but fails to reproduce the later part of the dynamics. The double exponential (green line) includes a much longer decay component and fits the entire decay. The time constant for the shorter decay is $t_1 \sim 0.6$ ps, whereas the time constant for the longer decay is $t_2 \sim 10$ ps, which is half of what is observed in the dephasing measurement. The circles are the experimental data.

for $\tau < 0$ ps, suggesting that some signal is observed for negative delays. This signal corresponds to the $k_A + k_B - k_C$ phase matching and is observed when pulse ordering is reversed with pulse A* arriving behind B and C.[43] The negative delay signal is thought to originate from many body interactions such as the two-exciton quantum coherence.[44,45]

In the FWM experiment, the exciton quantum dynamics is characterized by two fundamental parameters, the population decay time T_1 and the dephasing time T_2. The excited state population relaxation rate Γ is inversely proportional to the population decay time T_1. In a coherent experiment, the population relaxation rate Γ is thought to arise solely from the radiative recombination. The dephasing rate γ is inversely proportional to the dephasing time T_2. Thus, the longer dephasing component $\tau_2 = T_2/2 \sim 20$ ps provides the limit for the homogeneous broadening of excitons in $NiPS_3$ corresponding to a line width of <20 μeV.[21] To further investigate the mechanism of excitonic dephasing, we use a pulse sequence of circularly polarized laser pulses shown in Figure 5a. We first scan the time delay τ to measure the dephasing time, and the data is shown in Figure 5a. Surprisingly, the periodic oscillations observed using the linearly polarized laser pulses are suppressed, likely due to selection rules. In antiferromagnetic materials, the spins in each sublattice are aligned in the opposite direction. Circularly polarized light pulses may excite only one of the spin orientations, possibly failing to generate antiferromagnetic magnons. The remaining residual oscillations are likely due to a slight ellipticity of the laser pulses. The same behavior of the dephasing dynamics is observed as in Figure 4 for linearly polarized laser excitations. The same double exponential decay with time constants $\tau_1 \sim 1.2$ ps and $\tau_2 \sim 20$ ps is used to fit the experimental data, and it reproduces well the observed dynamics.

The population relaxation and the dephasing time are intimately linked, and usually the radiative recombination last longer than the dephasing time. The coherent superposition of the crystal ground and the exciton states determines the homogeneous line width of an excitonic resonance. The homogeneous line width is linked to population relaxation through $\gamma = \Gamma/2 + \gamma^*$, where γ^* characterizes pure dephasing processes such as elastic exciton−exciton and exciton−phonon scattering. Thus, T_1 and T_2 are established key ingredients for quantum optoelectronic devices and quantum information processing applications in semiconductors. Local potentials arising from defects and impurities shift the exciton energy and result in inhomogeneous distribution of exciton frequencies or inhomogeneous broadening. This type of spectral broadening conceals the intrinsic exciton homogeneous line width in low-temperature optical spectroscopy.[46]

To further investigate the role of the population relaxation, we measure it by scanning the time delay T between pulses A*/B and C and maintaining pulses A* and B at a temporal overlap. The data is shown in Figure 5b and is best reproduced by a double exponential fitting with time constants $t_1 \sim 0.6$ ps and $t_2 \sim 10$ ps. The population relaxation T_1 decays twice as fast as the dephasing T_2 and thus sets the limit for the coherence time. The mechanism of population relaxation is not clear. Tightly bound excitons with unscreened Coulomb interactions are expected to decay fast, within 1 ps. However, spin selection rules that are either partially forbidden or require wavevector conserving quasi-particles can prolong the lifetime. The shorter dephasing component of ~1.2 ps corresponds to a homogeneous line width of ~0.25 meV. This line width is comparable to the line widths observed in the absorption spectra of ~0.3 and ~0.4 meV and which are thought to be significantly inhomogeneously broadened due to their Gaussian line shapes. Thus, we conclude that this is not the dominating mechanism but likely caused by material properties such as defects and impurities which further reduce the radiative lifetime to ~0.6 ps. This behavior is unusual among

https://doi.org/10.1021/acsphotonics.5c01214
ACS Photonics 2025, 12, 5921−5928

excitons since in semiconductors the radiative life far exceeds the coherence time.

CONCLUSIONS

In conclusion, we performed magnetic field measurements up to 25 T to investigate the nature of the excitonic transitions in $NiPS_3$. Absorption spectroscopy reveals three subcomponents which had been previously observed. The absorption intensity depends strongly on the polarization of the incoming light. The large magnetic fields are used to orient the Neel vectors of the excitonic absorption. When the Neel vectors are oriented perpendicular to the electric field vector of the incoming light, the subcomponents of the excitonic transition saturate becoming equal intensity. The excitonic lines vanish when the polarization of the incoming light is parallel to the Neel vectors. This suggest that the excitonic subcomponents belong to equivalent excitons associated with three orientations of the Neel vector.

The central finding of this study is the measurement of the excitonic coherence in $NiPS_3$ and the mechanism limiting it. The excitonic dephasing was measured using FWM spectroscopy. The dephasing time T_2 is inversely proportional to the homogeneous line width, providing an upper limit for the homogeneous line width of <20 μeV. A shorter component was attributed to excitons affected by material imperfections such as crystal defects or impurities. Periodic oscillations are observed with a period of ∼0.85 ps, corresponding to an energy of ∼5 meV. This agrees well with optically active coherent magnons observed previously. The period of oscillations does not agree with the energy separation of the excitonic subcomponents. Furthermore, magnetic field studies indicate independent weakly interacting excitons.

ASSOCIATED CONTENT

Data Availability Statement

All data are available in the main text or the Supporting Information.

Supporting Information

The Supporting Information is available free of charge at https://pubs.acs.org/doi/10.1021/acsphotonics.5c01214.

Additional experimental details, materials, and methods, including additional drawing of the experimental setup (PDF)

AUTHOR INFORMATION

Corresponding Author

Denis Karaiskaj − *Department of Physics, University of South Florida, Tampa, Florida 33620, United States;* orcid.org/0000-0002-3181-7545; Email: karaiskaj@usf.edu

Authors

Sean Knapp − *Department of Physics, University of South Florida, Tampa, Florida 33620, United States*

Arup Barua − *Department of Physics, University of South Florida, Tampa, Florida 33620, United States*

Chevy Boegel − *Department of Physics, University of South Florida, Tampa, Florida 33620, United States*

Shirin Mozaffari − *Department of Materials Science and Engineering, University of Tennessee, Knoxville, Tennessee 37996, United States*

Matthew Cothrine − *Department of Materials Science and Engineering, University of Tennessee, Knoxville, Tennessee 37996, United States*

David Mandrus − *Department of Materials Science and Engineering, University of Tennessee, Knoxville, Tennessee 37996, United States;* orcid.org/0000-0003-3616-7104

Dmitry Semenov − *National High Magnetic Field Laboratory, Florida State University, Tallahassee, Florida 30201, United States*

Stephen A. McGill − *National High Magnetic Field Laboratory, Florida State University, Tallahassee, Florida 30201, United States*

Aldo H. Romero − *Department of Physics and Astronomy, West Virginia University, Morgantown, West Virginia 26506, United States;* orcid.org/0000-0001-5968-0571

Nihar Pradhan − *Layered Materials and Device Physics Laboratory, Department of Chemistry, Physics and Atmospheric Science, Jackson State University, Jackson, Mississippi 39217, United States;* orcid.org/0000-0002-3912-4233

Complete contact information is available at: https://pubs.acs.org/10.1021/acsphotonics.5c01214

Author Contributions

Conceptualization: DK, AHR, and SAM; methodology: DK, SM, MC, DM, DS, SAM, AHR, and NP; investigation: SK, AB, CB, SM, MC, DM, SAM, and DK; visualization: SK and DK; supervision: DK, SAM, and DM; writing—original draft: SK and DK; and Writing—review and editing: DK.

Notes

The authors declare no competing financial interest.

ACKNOWLEDGMENTS

A portion of this work was performed at the National High Magnetic Field Laboratory. The National High Magnetic Field Laboratory is supported by the National Science Foundation through NSF/DMR-2128556 and the State of Florida. S.M. and D.M. acknowledge the support from AFOSR MURI Grant No. FA9550-20-1-0322.

REFERENCES

(1) Burch, K. S.; Mandrus, D.; Park, J.-G. Magnetism in two-dimensional van der Waals materials. *Nature* **2018**, *563*, 47−52.

(2) Wildes, A. R.; Simonet, V.; Ressouche, E.; McIntyre, G. J.; Avdeev, M.; Suard, E.; Kimber, S. A. J.; Lançon, D.; Pepe, G.; Moubaraki, B.; Hicks, T. J. Magnetic structure of the quasi-two-dimensional antiferromagnet $NiPS_3$. *Phys. Rev. B* **2015**, *92*, 224408.

(3) Lançon, D.; Ewings, R. A.; Guidi, T.; Formisano, F.; Wildes, A. R. Magnetic exchange parameters and anisotropy of the quasi-two-dimensional antiferromagnet $NiPS_3$. *Phys. Rev. B* **2018**, *98*, 134414.

(4) Wildes, A. R.; Stewart, J. R.; Le, M. D.; Ewings, R. A.; Rule, K. C.; Deng, G.; Anand, K. Magnetic dynamics of $NiPS_3$. *Phys. Rev. B* **2022**, *106*, 174422.

(5) Kang, S.; et al. Coherent many-body exciton in van der Waals antiferromagnet $NiPS_3$. *Nature* **2020**, *583*, 785−789.

(6) Hwangbo, K.; Zhang, Q.; Jiang, Q.; Wang, Y.; Fonseca, J.; Wang, C.; Diederich, G. M.; Gamelin, D. R.; Xiao, D.; Chu, J.-H.; Yao, W.; Xu, X. Highly anisotropic excitons and multiple phonon bound states in a van der Waals antiferromagnetic insulator. *Nat. Nanotechnol.* **2021**, *16*, 655−660.

(7) Afanasiev, D.; Hortensius, J. R.; Matthiesen, M.; Mañas-Valero, S.; Šiškins, M.; Lee, M.; Lesne, E.; van Der Zant, H. S.; Steeneken, P. G.; Ivanov, B. A.; Coronado, E.; Caviglia, A. D. Controlling the

anisotropy of a van der Waals antiferromagnet with light. *Sci. Adv.* **2021**, *7*, No. eabf3096.
(8) Wang, X.; Cao, J.; Li, H.; Lu, Z.; Cohen, A.; Haldar, A.; Kitadai, H.; Tan, Q.; Burch, K. S.; Smirnov, D.; Xu, W.; Sharifzadeh, S.; Liang, L.; Ling, X. Electronic Raman scattering in the 2D antiferromagnet $NiPS_3$. *Sci. Adv.* **2022**, *8*, No. eabl7707.
(9) Wang, X.; Cao, J.; Lu, Z.; Cohen, A.; Kitadai, H.; Li, T.; Tan, Q.; Wilson, M.; Lui, C. H.; Smirnov, D.; Sharifzadeh, S.; Ling, X. Spin-induced linear polarization of photoluminescence in antiferromagnetic van der Waals crystals. *Nat. Mater.* **2021**, *20*, 964−970.
(10) Kim, D. S.; Huang, D.; Guo, C.; Li, K.; Rocca, D.; Gao, F. Y.; Choe, J.; Lujan, D.; Wu, T.; Lin, K.; et al. Anisotropic Excitons Reveal Local Spin Chain Directions in a van der Waals Antiferromagnet. *Adv. Mater.* **2023**, *35*, 2206585.
(11) Jana, D.; Kapuscinski, P.; Mohelsky, I.; Vaclavkova, D.; Breslavetz, I.; Orlita, M.; Faugeras, C.; Potemski, M. Magnon gap excitations and spin-entangled optical transition in the van der Waals antiferromagnet $NiPS_3$. *Phys. Rev. B* **2023**, *108*, 115149.
(12) He, W.; Shen, Y.; Wohlfeld, K.; Sears, J.; Li, J.; Pelliciari, J.; Walicki, M.; Johnston, S.; Baldini, E.; Bisogni, V.; Mitrano, M.; Dean, M. P. M. Magnetically propagating Hund's exciton in van der Waals antiferromagnet $NiPS_3$. *Nat. Commun.* **2024**, *15*, 3496.
(13) Zhang, F. C.; Rice, T. M. Effective Hamiltonian for the superconducting Cu oxides. *Phys. Rev. B* **1988**, *37*, 3759−3761.
(14) Collart, E.; Shukla, A.; Rueff, J.-P.; Leininger, P.; Ishii, H.; Jarrige, I.; Cai, Y. Q.; Cheong, S.-W.; Dhalenne, G. Localized and Delocalized Excitons: Resonant Inelastic X-Ray Scattering in $La_{2-x}Sr_xNiO_4$ and $La_{2-x}Sr_xCuO_4$. *Phys. Rev. Lett.* **2006**, *96*, 157004.
(15) Monney, C.; et al. Determining the Short-Range Spin Correlations in the Spin-Chain Li_2CuO_2 and $CuGeO_3$ Compounds Using Resonant Inelastic X-Ray Scattering. *Phys. Rev. Lett.* **2013**, *110*, 087403.
(16) Dirnberger, F.; Bushati, R.; Datta, B.; Kumar, A.; MacDonald, A. H.; Baldini, E.; Menon, V. M. Spin-correlated exciton−polaritons in a van der Waals magnet. *Nat. Nanotechnol.* **2022**, *17*, 1060−1064.
(17) Lane, C.; Zhu, J.-X. Thickness dependence of electronic structure and optical properties of a correlated van der Waals antiferromagnetic $NiPS_3$ thin film. *Phys. Rev. B* **2020**, *102*, 075124.
(18) Klaproth, T.; Aswartham, S.; Shemerliuk, Y.; Selter, S.; Janson, O.; van den Brink, J.; Büchner, B.; Knupfer, M.; Pazek, S.; Mikhailova, D.; Efimenko, A.; Hayn, R.; Savoyant, A.; Gubanov, V.; Koitzsch, A. Origin of the Magnetic Exciton in the van der Waals Antiferromagnet $NiPS_3$. *Phys. Rev. Lett.* **2023**, *131*, 256504.
(19) Nitsche, R.; Wild, P. Crystal growth of metal-phosphorus-sulfur compounds by vapor transport. *Mater. Res. Bull.* **1970**, *5*, 419−423.
(20) Paul, J.; Stevens, C. E.; Smith, R. P.; Dey, P.; Mapara, V.; Semenov, D.; McGill, S. A.; Kaindl, R. A.; Hilton, D. J.; Karaiskaj, D. Coherent two-dimensional Fourier transform spectroscopy using a 25 Tesla resistive magnet. *Rev. Sci. Instrum.* **2019**, *90*, 063901.
(21) Shah, J. *Ultrafast Spectroscopy of Semiconductors and Semiconductor Nanostructures*; Springer-Verlag, 1999.
(22) Cundiff, S. T. Coherent spectroscopy of semiconductors. *Opt. Express* **2008**, *16*, 4639.
(23) Mapara, V.; et al. Bright and Dark Exciton Coherent Coupling and Hybridization Enabled by External Magnetic Fields. *Nano Lett.* **2022**, *22*, 1680−1687.
(24) Mapara, V.; Stevens, C. E.; Paul, J.; Barua, A.; Reno, J. L.; McGill, S. A.; Hilton, D. J.; Karaiskaj, D. Multidimensional spectroscopy of magneto-excitons at high magnetic fields. *J. Chem. Phys.* **2021**, *155*, 204201.
(25) Stevens, C. E.; Paul, J.; Cox, T.; Sahoo, P. K.; Gutiérrez, H. R.; Turkowski, V.; Semenov, D.; McGill, S. A.; Kapetanakis, M. D.; Perakis, I. E.; Hilton, D. J.; Karaiskaj, D. Biexcitons in monolayer transition metal dichalcogenides tuned by magnetic fields. *Nat. Commun.* **2018**, *9*, 3720.
(26) Stevens, C. E.; Dey, P.; Paul, J.; Wang, Z.; Zhang, H.; Romero, A.; Shan, J.; Hilton, D.; Karaiskaj, D. The role of electron-phonon interactions on the coherence lifetime of monolayer transition metal dichalcogenides. *Solid State Commun.* **2017**, *266*, 30.
(27) Paul, J.; Stevens, C. E.; Zhang, H.; Dey, P.; McGinty, D.; McGill, S. A.; Smith, R. P.; Reno, J. L.; Turkowski, V.; Perakis, I. E.; Hilton, D. J.; Karaiskaj, D. Coulomb-interaction induced coupling of Landau levels in intrinsic and modulation-doped quantum wells. *Phys. Rev. B* **2017**, *95*, 245314.
(28) Dey, P.; Paul, J.; Wang, Z.; Stevens, C. E.; Liu, C.; Romero, A. H.; Shan, J.; Hilton, D. J.; Karaiskaj, D. Optical Coherence in Atomic-Monolayer Transition-Metal Dichalcogenides Limited by Electron-Phonon Interactions. *Phys. Rev. Lett.* **2016**, *116*, 127402.
(29) Paul, J.; Stevens, C. E.; Liu, C.; Dey, P.; McIntyre, C.; Turkowski, V.; Reno, J. L.; Hilton, D. J.; Karaiskaj, D. Strong Quantum Coherence between Fermi Liquid Mahan Excitons. *Phys. Rev. Lett.* **2016**, *116*, 157401.
(30) Dey, P.; Paul, J.; Moody, G.; Stevens, C. E.; Glikin, N.; Kovalyuk, Z. D.; Kudrynskyi, Z. R.; Romero, A. H.; Cantarero, A.; Hilton, D. J.; Karaiskaj, D. Biexciton formation and exciton coherent coupling in layered GaSe. *J. Chem. Phys.* **2015**, *142*, 212422.
(31) Dey, P.; Paul, J.; Glikin, N.; Kovalyuk, Z. D.; Kudrynskyi, Z. R.; Romero, A. H.; Karaiskaj, D. Mechanism of excitonic dephasing in layered InSe crystals. *Phys. Rev. B* **2014**, *89*, 125128.
(32) Paul, J.; Dey, P.; Tokumoto, T.; Reno, J. L.; Hilton, D. J.; Karaiskaj, D. Exploring two-dimensional electron gases with two-dimensional Fourier transform spectroscopy. *J. Chem. Phys.* **2014**, *141*, 134505.
(33) Bristow, A. D.; Karaiskaj, D.; Dai, X.; Zhang, T.; Carlsson, C.; Hagen, K. R.; Jimenez, R.; Cundiff, S. T. A versatile ultrastable platform for optical multidimensional Fourier-transform spectroscopy. *Rev. Sci. Instrum.* **2009**, *80*, 073108.
(34) Dey, P.; Paul, J.; Bylsma, J.; Deminico, S.; Karaiskaj, D. Continuously tunable optical multidimensional Fourier-transform spectrometer. *Rev. Sci. Instrum.* **2013**, *84*, 023107.
(35) Belvin, C. A.; Baldini, E.; Ozel, I. O.; Mao, D.; Po, H. C.; Allington, C. J.; Son, S.; Kim, B. H.; Kim, J.; Hwang, I.; Kim, J. H.; Park, J.-G.; Senthil, T.; Gedik, N. Exciton-driven antiferromagnetic metal in a correlated van der Waals insulator. *Nat. Commun.* **2021**, *12*, 4837.
(36) Ergeçen, E.; Ilyas, B.; Mao, D.; Po, H. C.; Yilmaz, M. B.; Kim, J.; Park, J.-G.; Senthil, T.; Gedik, N. Magnetically brightened dark electron-phonon bound states in a van der Waals antiferromagnet. *Nat. Commun.* **2022**, *13*, 98.
(37) Toyoda, S.; Kruppe, J.; Yamakawa, K.; Analytis, J.; Orenstein, J. Phase control of spin waves in the van der Waals antiferromagnet $NiPS_3$. *Phys. Rev. B* **2024**, *109*, 064408.
(38) Schultheis, L.; Kuhl, J.; Honold, A.; Tu, C. W. Ultrafast Phase Relaxation of Excitons via Exciton-Exciton and Exciton-Electron Collisions. *Phys. Rev. Lett.* **1986**, *57*, 1635.
(39) Leo, K.; Wegener, M.; Shah, J.; Chemla, D. S.; Göbel, E. O.; Damen, T. C.; Schmitt-Rink, S.; Schäfer, W. Effects of coherent polarization interactions on time-resolved degenerate four-wave mixing. *Phys. Rev. Lett.* **1990**, *65*, 1340.
(40) Leo, K.; Shah, J.; Göbel, E. O.; Damen, T. C.; Schmitt-Rink, S.; Schäfer, W.; Köhler, K. Coherent oscillations of a wave packet in a semiconductor double-quantum-well structure. *Phys. Rev. Lett.* **1991**, *66*, 201.
(41) Lyssenko, V. G.; Erland, J.; Balslev, I.; Pantke, K.-H.; Razbirin, B. S.; Hvam, J. M. Nature of nonlinear four-wave-mixing beats in semiconductors. *Phys. Rev. B* **1993**, *48*, 5720.
(42) Bylsma, J.; Dey, P.; Paul, J.; Hoogland, S.; Sargent, E. H.; Luther, J. M.; Beard, M. C.; Karaiskaj, D. Quantum beats due to excitonic ground-state splitting in colloidal quantum dots. *Phys. Rev. B* **2012**, *86*, 125322.
(43) Mukamel, S. *Nonlinear Optical Spectroscopy*; Oxford University Press, 1995.
(44) Chemla, D. S.; Shah, J. Many-body and correlation effects in semiconductors. *Nature* **2001**, *411*, 549.
(45) Karaiskaj, D.; Bristow, A. D.; Yang, L.; Dai, X.; Mirin, R. P.; Mukamel, S.; Cundiff, S. T. Two-Quantum Many-Body Coherences in Two-Dimensional Fourier-Transform Spectra of Exciton Reso-

https://doi.org/10.1021/acsphotonics.5c01214
ACS Photonics 2025, 12, 5921−5928

nances in Semiconductor Quantum Wells. *Phys. Rev. Lett.* **2010**, *104*, 117401.
(46) Moody, G.; Kavir Dass, C.; Hao, K.; Chen, C.-H.; Li, L.-J.; Singh, A.; Tran, K.; Clark, G.; Xu, X.; Berghauser, G.; Malic, E.; Knorr, A.; Li, X. Intrinsic homogeneous linewidth and broadening mechanisms of excitons in monolayer transition metal dichalcogenides. *Nat. Commun.* **2015**, *6*, 8315.

https://doi.org/10.1021/acsphotonics.5c01214
ACS Photonics 2025, 12, 5921−5928